Proposal of Bridge Features for Advanced Bridge Health Monitoring System
(橋梁ヘルスモニタリングシステム高度化のための橋梁特徴量の提案)

Principal Investigator: Dr. Gen HAYASHI,
Asst. Professor, Osaka Metropolitan University
研究代表者　大阪公立大学大学院工学研究科　助教　林 厳

1. Introduction

Constructed in the 1960s and the 1970s, a significant inventory of Japanese bridges are now aging. Consequently, the number of bridges in service for extended periods is projected to increase significantly in the future[1]. The 2014 revision of the periodic bridge inspection guidelines man dated a five-year inspection for each bridge in Japan. According to inspections conducted across Japanese bridges up to 2018, approximately 59% of them exhibited some form of damages, which is expected to increase with the ongoing ageing of these structures. The deteriorating of these bridges is a global issue, with numerous instances of structural damage and bridge collapse owing to misjudgment in the inspection process having been reported. In 2019, Nanfangao Bridge[2] experienced a collapse, followed by the collapse of the Musota Aqueduct Bridge[3] in 2021. Against this background, vibration-based structural health monitoring (VSHM), which utilises the vibration response of bridges as a straightforward and effective diagnostic tool, has gained momentum[4,5,6,7,8].

Truss bridges and arch bridges are susceptible to significant impacts on the overall stability of the structure by damages. Therefore, extensive research has been conducted on them. Varing the bridge response, damage to the main members is anticipated, leading to investigations into methods that use features such as natural frequencies identifiable from the response acceleration due to vehicular and ambient vibrations. For truss bridge, Kim et al. [9,10] conducted vibration experiments by cutting members of real bridge after service. For arch bridge, vibration experiments and numerical simulation was conducted on model bridges[11,12,13]. These studies suggest the possibility of anomaly detection at the member rupture level, highlighting the potential advantages of VSHM for redundant bridge structures.

The estimation of the damage location and extent is vital for an efficient VSHM. Lee et al. proposed an entropy-based method for locating damage in truss bridges using a continuous wavelet transform[14], thus demonstrating the potential for both damage detection and multiple damage location estimation. Zhang et al. demonstrated that the running load from a single truck can be integrated with the bridge weigh-in-motion

(BWIM) algorithm, utilising the rotation angle of the bearings for estimating the vehicle weight and detecting damage in PC girder bridges[15]. Huseynov et al. theoretically and empirically illustrated the possibility of estimating the damage location and identifying the damage level for singular damage instances by using influence lines from the rotation angle along the bridge axis obtained via tiltmeters installed at various bridge locations[16].

Despite efforts in damage detection using the vibration characteristics and rotation angles independently, few studies have sought to combine these techniques for enhancing the sophistication of bridge health monitoring. Furthermore, bridges with numerous joints, such as truss and arch bridges, may have multiple members damaged within areas that are difficult for visual inspection. However, past studies have focused on multiple damage detection methods that require multi-point observations for location estimation. It is crucial to understand the mechanical behaviour of the bridge with damages, particularly when the number of sensors is limited, for a straightforward structural monitoring method.

To address these challenges, this study explores the applicability of VSHM to a model Langar arch bridge in terms of vibration characteristics and rotation angle under the condition of anomaly detection with a limited number of sensors. This approach has rarely been adopted previously. First, a finite element (FE) model of the target bridge was developed in which the simulated damages by varying the damaged member, location, and level. The variations in the mechanical behaviour and vibration characteristics of the steel arch bridge with damage were analysed. The changes in natural frequencies and rotation angles were then quantitatively evaluated. Subsequently, various damage scenarios involving different combinations of single-and multiple (two-location) damage instances were analysed. The aim was to clarify the mechanisms driving changes in the mechanical behaviour and natural frequencies of the bridge and investigate the potential for damage detection with a small number of sensors.

2. Research methods

2.1. Target bridges

The subject of this study was a 1/15 scale model of a 75-m-long Langer arch bridge, as depicted in Figure 1, 2. Dimensions of the bridge model are 5000 mm in length, 567 mm in width, and 893 mm in height, and comprised stiffening girders, arch ribs, cross girders, hangers, and gusset plates made of SS400 (JIS G 3101) plates. The cross-sectional shapes and dimensions of these components are presented in Table 1.

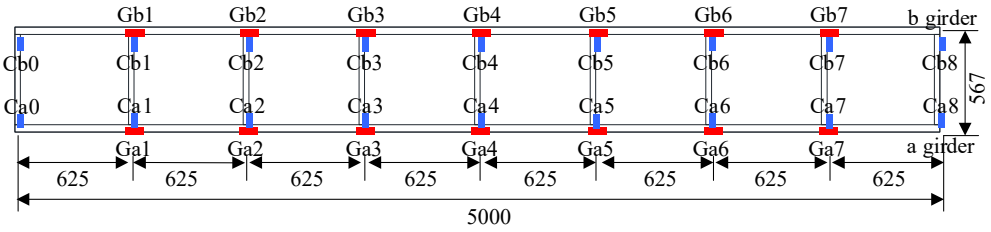

(a) Bottom plane view

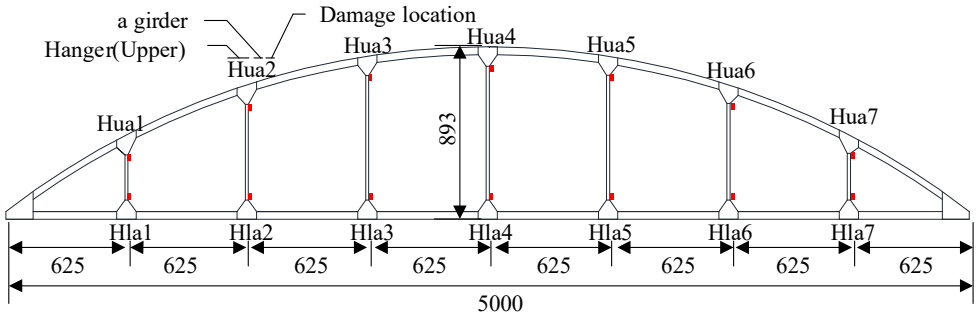

(b) A side Plane view

Figure 1 Dimensions of the target bridge and damage location. (Unit: mm)

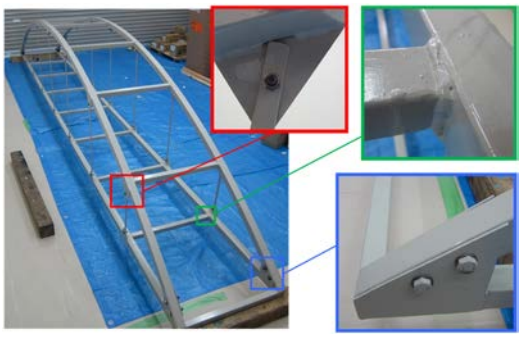

Figure 2 Joints of langer arch bridge

Table 1 Dimensions of members

Member	$(b \times h \times t)$ (mm)	Cross section
Stiffening girder	40×40×1.6	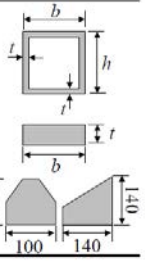
Arch rib	40×40×2.0	
Cross girder	30×30×1.6	
Hanger	16(b)×4.5(t)	
Gusset	t=3	

Connections between members were made with M6 bolts via gusset plates for the hanger members and stiffening girders/arch ribs and M8 bolts via those for the connections between the arch ribs and stiffening girders.

2.2. FE model

Figure 3 presents an analytical model of a bridge constructed using Abaqus/Explicit 2022 [17]. All the members were modelled by beam elements, with the boundary conditions set as the pin and roller supports. Since the actual modelled bridge was bolted via gussets shown in Figure 2, the connections between the members were assumed fully connected. The element divisions were 250 for arch ribs and stiffening girders, 30

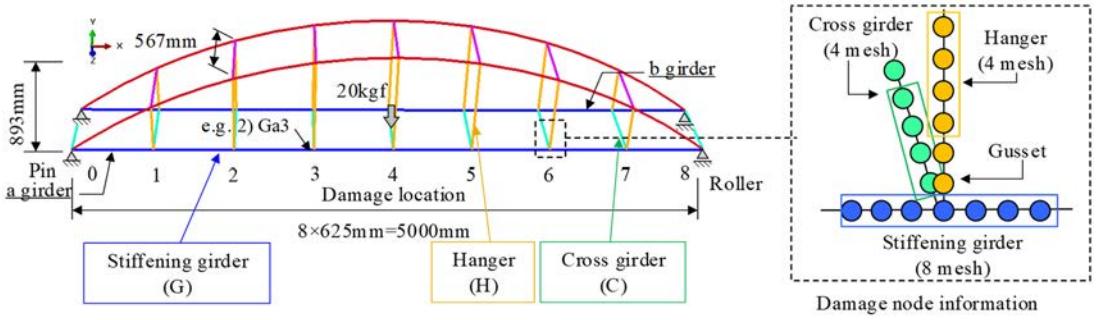

Figure 3 Analytical model and loading position

for cross girders, and 20–40 for hanger members, depending on their lengths. The damage analysis was performed by reducing the cross-sectional area of each joint. The element divisions of damage were three. The material properties of the members were as follows: elastic modulus of 200 kN/mm^2, Poisson's ratio of 0.3, density of 77 kN/m^3, and total weight of 65 kg, which were identical to those of the model bridge. The section of the gusset plate connected to the hanger members were modelled by adjusting the cross-section of the beam element to match the dimensions of the gusset plate. The gusset plates between the stiffening girders and arch ribs were represented by increasing their elastic modulus to 370 kN/mm^2.

2.3. Damage scenario

The damage was set at the coloured positions indicated in Figure 1. The damage was presumed to be localised corrosion of the hangers and internal corrosion at various points on the cross and stiffening girders.

The damaged members were the connecting points of the stiffening girder (G), hanger members (Hl: lower, Hu: upper), and cross girder (C), as illustrated in the coloured sections of Figure 1. Damage labelling follows the pattern 'member name (G, Hl, Hu, C) + girder name (a, b) + damage location (0-8) shown as Figure 1.

The damage scenarios are presented in Table 2. For the single-damage scenarios, there were 180 cases (60 locations 3 levels = 180 cases). Damage levels of 25, 50, and 75% were applied to 60 locations across the stiffening girders,× hanger members, and cross girders. For the multiple-damage scenarios, 78 patterns were selected from the 13 locations that were most prone to damage among the single-damage cases, and these were combined, as shown in Table 2. This resulted in 702 cases (78 × 9 damage patterns).

Table 2 Damage scenario

	Damage name	Damage level (%)		Damage1 name	Damage2 name	Damage1 level (%)	Damage2 level (%)
Single damage	Ga1~Ga7	25 50 75	Multiple damage	Gb4	Gb4	25 50 75	25 50 75
	Gb1~Gb7			Gb6	Gb6		
	Hla1~Hla7			Gb7	Gb7		
	Hlb1~Hlb7			Hla3	Hla3		
	Hua1~Hua7			Hla5	Hla5		
	Hub1~Hub7			Hlb3	Hlb3		
	Ca0~Ca8			Hua6	Hua6		
	Cb0~Cb8			Hub2	Hub2		
				Hub3	Hub3		
				Ca2	Ca2		
				Ca3	Ca3		
				Ca4	Ca4		
				Cb7	Cb7		

2.4. Analysis method

In the damage analysis, both eigenvalue and static analyses were conducted. In eigenvalue analysis, the focus is on identifying modes that can be measured in model experiments actually conducted. The natural frequencies of the first-to third-order bending modes and first-to second-order transverse modes along the longitudinal axis were extracted from the effective mass of the analysis results. The static analysis involved a linear elastic analysis with a concentrated load (20 kN) applied at the centre of the span, as depicted in Figure 3. It was assumed that the rotation angles could be measured using triaxial accelerometers and gyro sensors on an actual bridge. Thus, the rotation angles around the x axis (longitudinal direction) and z axis (transverse direction) at the midsection of the cross girder in the span centre (loading point) were extracted. The unit of rotation angles is degrees (°), with the positive direction being clockwise.

3. Single damage

3.1. Eigenvalue analysis results

Figure 4 shows the natural frequencies of the first-to third-order bending modes and first- and second-order transverse modes in the intact case (INT) obtained from the analysis, along with the natural frequencies of these modes. Figure 5 shows the mode shapes when Hlb3 was damaged as an example. In this way, it was confirmed that, even with the damages, the mode shapes did not change. Figure 6 shows the damage location and difference between the natural frequencies of the intact and damaged cases. The

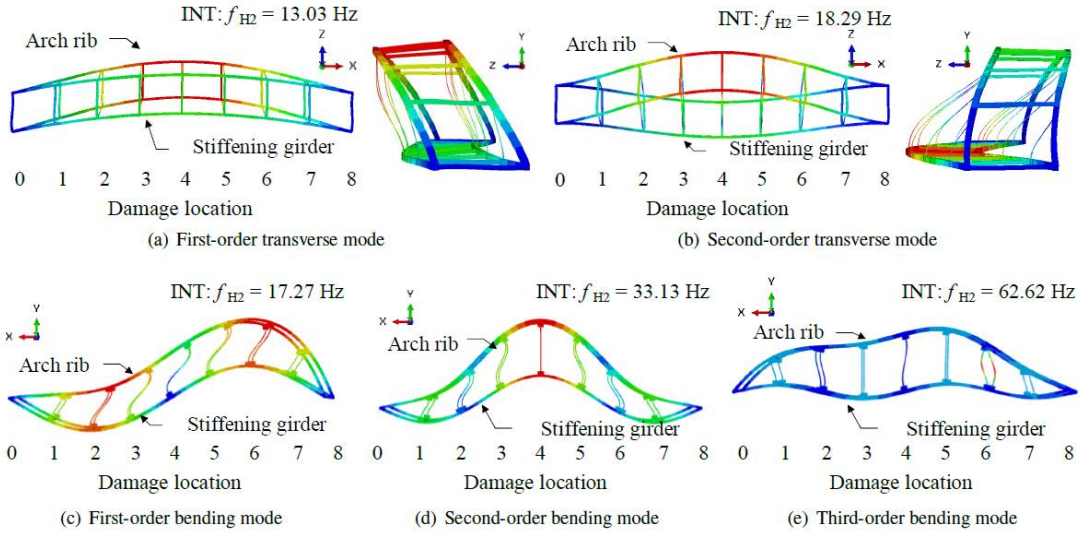

Figure 4 Natural vibration modes

Figure 5 Natural vibration modes at single damage

horizontal axis represents the damage location, as shown in Figure 1, and the vertical shows the change in the natural frequency for each vibration mode. A negative value on the vertical axis indicates a decrease in the natural frequency. Because the trend was similar in all cases, the damage level for a single damage shown in the figure is represented only by the 75% damage case because the difference is only in the natural frequency.

For the first-order transverse mode, as depicted in Figure 6(a), the natural frequency changed by only a few Hertz when the near L/4 of stiffening girders (damage locations 1, 2, 6, and 7) were damaged. However, when the cross-girders at the bearing locations (damage locations 0 and 8) were damaged, the natural frequency significantly changed. This change is asymmetric with respect to the centre of the span, with a greater decrease observed when the damage is on the pin bearing side. Conversely, the natural frequency barely changed when the central cross-girders were damaged, and the reduction rate of the damage to the cross girders near the roller bearing was smaller than that on the pin bearing side. In essence the first-order transverse mode is more significantly influenced by boundary conditions. The natural frequency decreased because of the stiffness

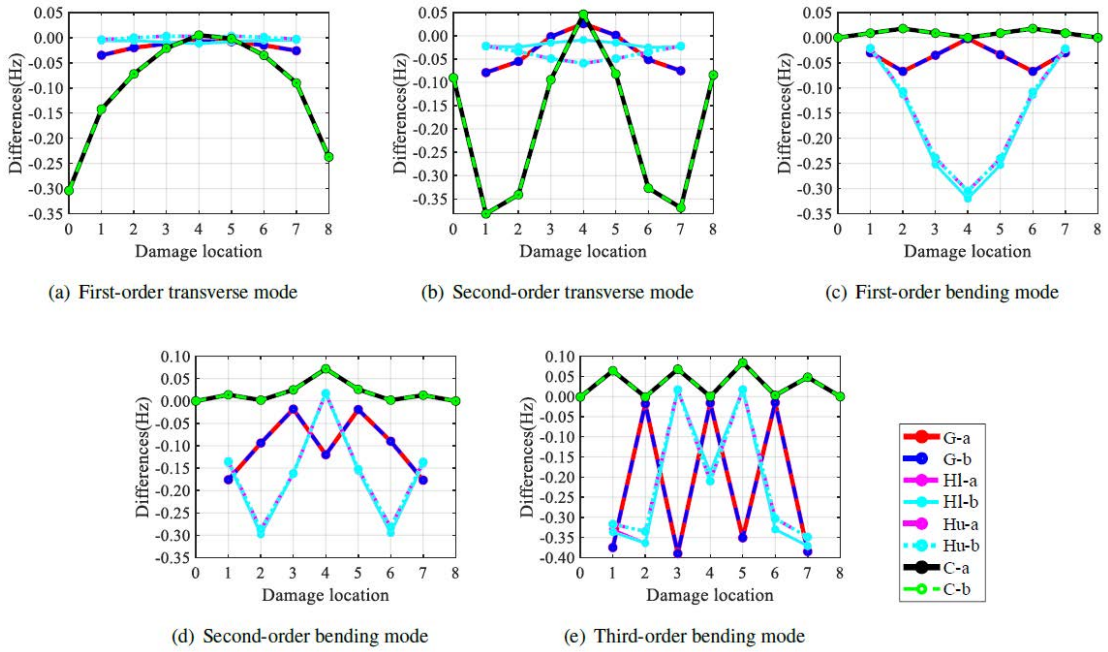

Figure 6 Relationship between damaged location and difference of natural frequencies (Damage level: 75%)

reduction caused by damage to the bridge end parts. This agrees with a previous study on girder bridges[18], which reported the impact of bridge edge damage on transverse vibration modes, and a similar trend was also observed for arch bridges.

In the second-order transverse mode, Figure 6(b) shows the effects of damage to both the hanger members and stiffening girders. Damage to the cross-girders significantly affects this mode. Unlike the first-order transverse mode, the natural frequencies exhibited substantial changes when the damage occurred near L/4 (damage positions 1, 2, 6, and 7). This is likely due to a stiffness of near L/4, given that the vibration mode causes twisting of the arch ribs and stiffening girders, as shown in Figure 4. Thus, it is suggested that damage to the cross-girder is more likely to influence the transverse vibration mode.

For the bending vibration mode, Figure 6(c) and (d) indicate that damage to the hanger members and stiffening girders significantly impacts these modes. This is likely because the stiffness of the stiffening girder contributes significantly to the vertical vibration. Moreover, that of the arch rib at the location of the damage influences the natural frequency owing to the substantial deformation of the vibration mode in the hanger members that connect the arch rib and stiffening girder.

In the first-order bending mode, the hanger member at damage locations 4 exhibits a higher degree of deformation during natural vibration. This is likely because the

differences in the vertical mode vectors of the stiffening girders and arch ribs at the nodal locations of the vibration mode were the largest. Moreover, the deformation of the hanger member prompted a bending vibration mode. This suggests that the stiffness of the hanger member contributes significantly to this mode of vibration, resulting in a larger change in the natural frequency when the hanger member is damaged at this location, as shown in Figure 6(c).

For the second-order bending mode, the changes in the natural frequency follow a similar pattern to those of the first-order bending mode in Figure 6(d). The change in natural frequencies is substantial at damage locations 2 and 6, where deformations are significant.

Furthermore, in the third-order bending mode, a similar trend is observed, with significant changes in natural frequencies at damage locations 2 and 6 in Figure 6(e).

The results for Hl and Hu indicate that the damage location within the hanger member was generally the same, suggesting that the damage location did not significantly influence the outcome if damage occurred within the same hanger member.

In contrast, the change in natural frequency owing to damage to the stiffening girder was found to be more significant when damage occurred at a location where the local vibration of the hanger member was minimal for both bending vibration modes. The position where the bending vibration of the stiffening girder becomes dominant is found to correspond to the belly position of the overall mode.

The above results reveal that the natural frequency of each vibration mode is contingent on both the location and member. However, it is important to note that the results for damage locations–0-4 and 4-8 (in the width direction of the bridge on the a- and b-sides, respectively) and at the target location centred around the middle of the bridge span were nearly identical. It is difficult to identify damage locations solely based on natural frequencies.

3.2. Static analysis results

The rotation angles around the x- and z-axes for each damage case in the damage analysis are shown in Figure 7. The horizontal axis represents the damage location, and the vertical axis represents the rotation angle. In accordance with the Cartesian coordinate system illustrated in Figure. 3, the rotation angle is positive in the clockwise direction. It is important to note that as shown in Figure 7(a), the positive and negative directions of rotation differ for girders a and b. Figure 8 shows an example of the deformation diagram under static loading with damage to Ga4 and Hla3.

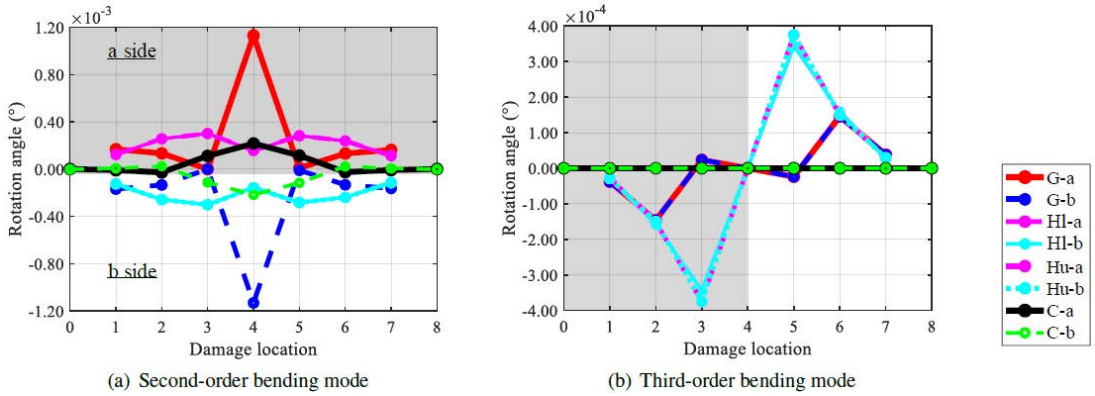

(a) Second-order bending mode (b) Third-order bending mode

Figure 7 Relationship between damaged location and rotations (Eigenvalue analysis)

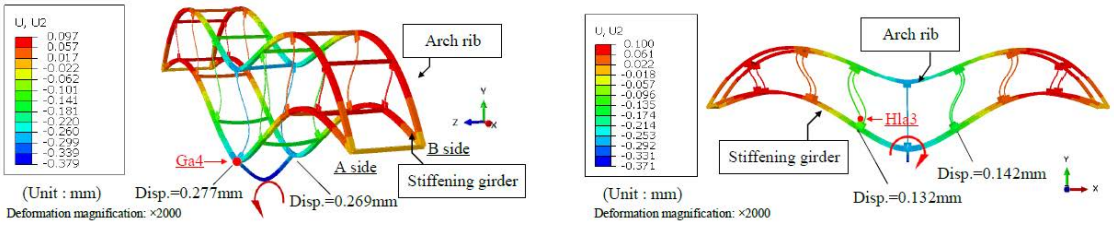

(a) Around x-axis (b) Around z-axis

Figure 8 Relationship between damaged location and rotations (Static analysis)

Figure 8(a) shows that the displacement of the stiffening girder under loading was greater for the damaged a-girder than for the undamaged b-girder. Therefore, it is believed that rotation around the x-axis likely tilts in the direction of damage. Thereby the rotation angle if the damage is located at a-girder becomes positive, while the rotation angle if the damage located at b-girder becomes negative. From these results, it can be observed in Figure 7(a) that the rotation angle can provide an estimation of the damage location if other members are damaged. However, the rotation angle changes minimally if the damage is located at positions 3 and 5 of the cross-girder and stiffening girder at the bridge end.

As shown in Figure 7(b), the damage locations in the longitudinal direction differed depending on whether the hanger member or stiffening girders were damaged. Specifically, differences were evident at the damage locations 0-4 and 4-8. The deformation diagram in Figure 8(b) represents a case in which there is a significant change in the rotation angle in the longitudinal direction. When a hanger member is damaged, the deflection immediately below the damaged member location is smaller than that at the symmetrical location with respect to the centre of the span, thereby

tilting it in the opposite direction of the damaged member.

The results above suggest that the rotation angle could potentially be used to estimate the location of damage in both the width direction (a- or b-girder) and longitudinally at the centre of the span (damage locations 0-4 and 4-8). These locations cannot be ascertained through the natural frequency alone. However, damage to the cross-girders located at the edge of the bridge seems to have a minimal impact on the rotation angle response, suggesting that other response values may need to be considered.

3.3. Damage location and damage level

In this section, the effects of varying damage levels from individual incidents on the natural frequency and rotational angular response are investigated.

Figure 9 presents the natural frequencies of the second-order transverse, first-order bending, and third-order bending modes, as well as the differences in rotation angles. In these figures, only damages at positions 0-4 of the A girder were considered. The damage levels taken into account were 25%, 50%, and 75%.

In Figure 9(a) and (b), the axes indicate the difference in frequency from the intact case for each natural-order bending mode in the damaged case. Specifically, Figure 9(a) shows the second-order transverse mode on the horizontal axis and the second-order bending mode on the vertical axis. In Figure 9(b), the second-and third-order bending modes are on the horizontal and vertical axes, respectively.

Finally, the axes in Figure 9(c) represent the difference in rotation angle relative to the intact case. The rotation angle in the longitudinal direction (x-axis) is shown on the horizontal axis, and that in the transverse direction (z-axis) on the vertical axis.

In all figures, the damaged members are represented by the colour of the plot (green for stiffening girders, orange for hanger members, and blue for cross girders), and the damage level is indicated by the marker shape (◯ for 25%, □ for 50%, and △ for 75%). The solid lines in the figure connected the points at the intact condition (0%) and 75% damage level.

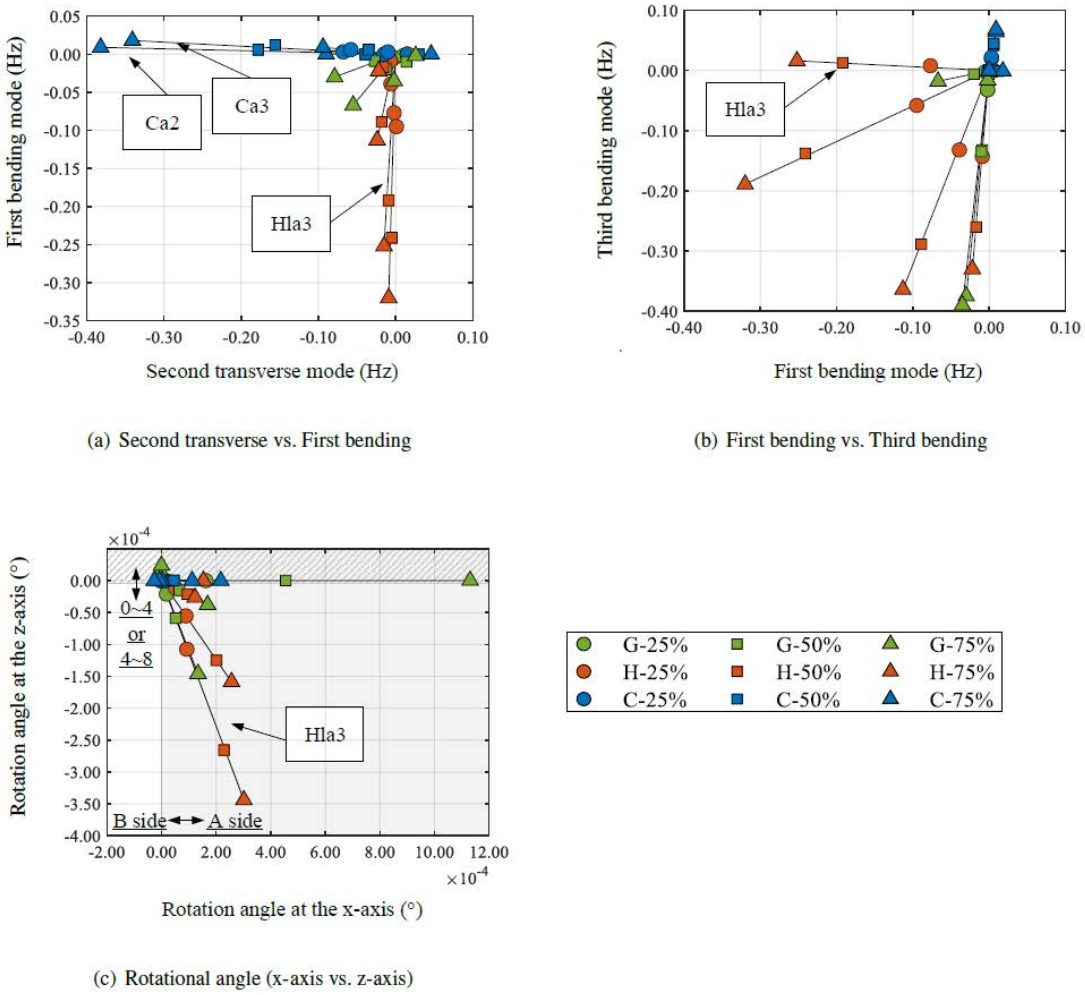

(a) Second transverse vs. First bending

(b) First bending vs. Third bending

(c) Rotational angle (x-axis vs. z-axis)

Figure 9 Relationship between damaged members / damage degree and natural frequencies / rotational angle

From the discussion on damage experiments on actual bridges in previous studies, it is known that the bearing conditions (boundary conditions) influence the vibration frequencies of each natural vibration mode differently. Therefore, the natural vibration modes selected for this study are those that are less affected by varying bearing conditions and more sensitive to damage, as revealed from the discussion in the previous section. Therefore, we focused on the second-order transverse mode, first-order bending mode and third-order bending mode that the influence of boundary conditions are small.

First, focusing on the relationship between the second-order transverse mode and first-order bending mode, we can discern from Figure 9(a) that the damage to Ca2 and Ca3 in the cross-girder causes significant changes in the x-axis direction, even though some damage points near the origin may appear indistinguishable. Damage to the hanger members induces variations in the y-axis direction, whereas that to the

stiffening girders causes changes in the direction oriented 45◦. Given these relationships, it is possible to estimate the damage location.

The relationship between the first- and third-order bending modes, as depicted in Figure 9(b), implies that the angle to the x-axis differs depending on the location of the hanger member damage. Hence, it may be possible to estimate the damage location based on this relationship.

Furthermore, the relationship between the rotation angles in Figure 9(c). In this figure, the rotation angle was positive around the x-axis and negative around the z-axis because the damaged member was located at damage locations 0-4 of girder A.

Distinctions among the damage levels were made evident by the near-linear alignment of plots for the three predefined damage levels in this study. This indicates that regardless of variations in the damage level, the damage to each member manifests in a specific natural frequency mode. Furthermore, the degree of change in the natural frequency increases with the damage level.

Figure 10 presents the results of a damage analysis conducted to further elucidate the relationship between damage level and the change in natural frequency. We focused on Hla3, for which a slight deviation from linearity was observed upon damage, as shown in Figure 10(a). The analysis was conducted at seven different damage levels: 6.25%, 12.5%, 25%, 37.5%, 50%, 62.5%, and 75%. The axes in the figures shown in Figure 10 represent the difference in the natural frequency relative to the intact condition, similar to Figure 8(a) and (b).

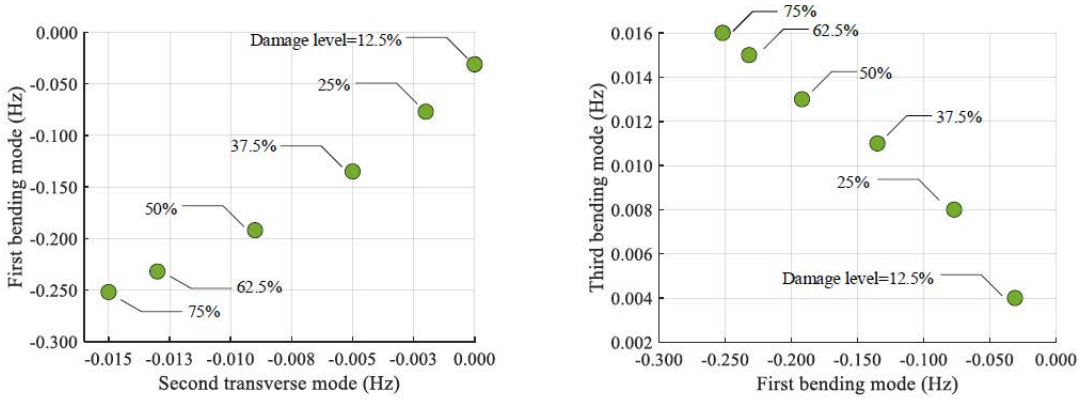

(a) Second transverse vs. First bending

(b) First bending vs. Third bending

Figure 10 Relationship between damage degree and natural frequencies in Hla3

In both Figure 10(a) and (b), it can be observed that the change in natural frequency maintains an almost linear that it may be possible to predict damage at unknown levels using natural frequencies.

4. Multiple damage

4.1. Change in natural frequency under multiple-damage

The results of plotting the differences in natural frequencies for each vibration mode in the multiple damage cases, as presented in Figure 2, are shown in Figure 11.

Furthermore, the first- and third-order bending modes for single and multiple damage are shown in Figure 12. For instance, Figure 11(a) illustrates the difference in the natural frequencies from those of the intact case for the first- and third-order bending modes. This applies to cases where Ga4, Hlb3, and Ga4+Hlb3 undergo damage across three damage stages.

From Figure 11(a), it is observed that in the cases of singular damage, either Ga4 (green) or Hlb3 (orange), the natural frequency changes linearly with the increasing damage level, as discussed in the Section3.3. In contrast, in the case of multiple damage instances, when the damage levels of Ga4 and Hlb3 were both 75% (Ga4:75%, Hlb3:75%), the change in natural frequency appeared to be the sum of the differences in natural frequencies between the 75% case for Ga4 damage and that for Hlb3 damage. In essence, in cases of multiple damage, the natural frequency changes in the coloured area of Figure 11(a). Therefore, the superposition of the results from singular damage instances may be utilised to estimate the damaged member and location of the damage. Figure 12 shows the mode shapes when multiple damages occur. From this figure, it is evident that there is minimal change in the mode shapes even when multiple damages occur. From this, it can be inferred, as described in Section 3.1, that the members or positions with significant deformation in each mode shape are the same. In other words, since the components and positions that have a large effect on the natural frequency of each mode are the same as a single damage, the change in natural frequency can be considered as the sum of the effects of individual damage on each mode. This trend was similarly observed for other damages.

Similarly, other members were studied, and the results of the 3D plot are shown in Figure 11(b). The figure indicates the same trend observed for the Ga4 and Hlb3 damage cases applies to other combinations of damage cases, with the distributions clustered on the same plane.

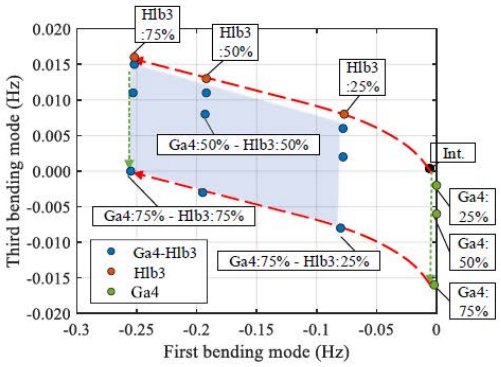

(a) Single/multiple damage of stiffening girders

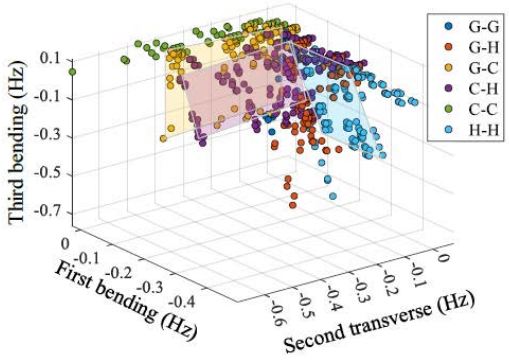

(b) 3-D distribution of natural frequencies of damaged cases

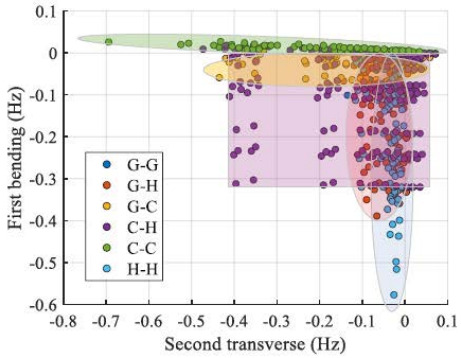

(c) Second transverse vs. First bending

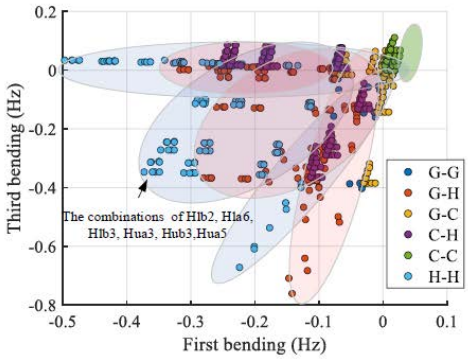

(d) First bending vs. Third bending

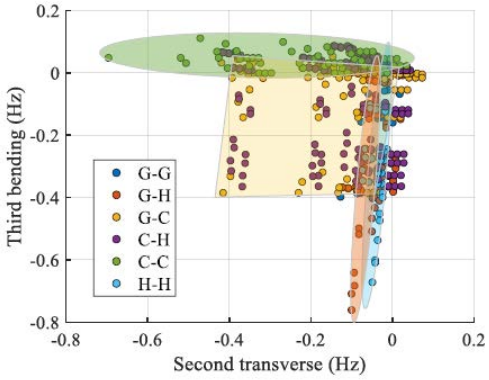

(e) Second transverse vs. Third bending

Figure 11 Differential natural frequencies for each vibration mode in multiple damage cases

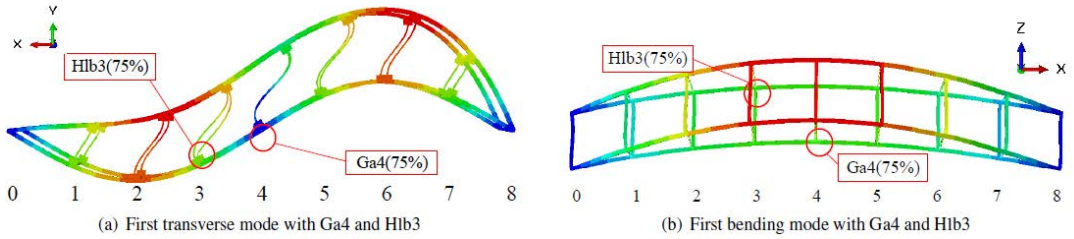

(a) First transverse mode with Ga4 and Hlb3 (b) First bending mode with Ga4 and Hlb3

Figure 12 Natural vibration modes with multiple damage

4.2. Damaged member/location vs. natural frequency.

Figure 11(c)-(e) present the results of 2D plots on each axis plane derived from the 3D plot of Figure 11(b). The aim was to investigate the applicability of damage-detection methods based on changes in the frequencies of the characteristic natural vibration modes for multiple damage relationship when the level of damage varies. From the relationship observed between the curves, it can be inferred scenarios, as detailed in Figure 11(a). It is important to note that Figure 11(c)–(e) also show plots of the combinations of damaged members with varying marker shapes and plane colours.

Figure 11(c) illustrates the relationship between the natural frequencies of the second-order transverse mode and the first-order bending mode. Combinations of damaged members typically demonstrate cohesiveness of the same colour. Notably, in the case of combinations of the same members, the influence on the specific vibration modes is particularly pronounced. The cross girder exhibited a significant impact on the second-order transverse mode, while the hanger member had a pronounced effect on the first-order bending mode. Consequently, notable changes in the frequencies of the second-order transverse mode in the combination of cross girders (C-C) and first-order bending mode in the combination of hanger members (H-H) were observed.

This is evidenced by the changes in the natural frequencies of the first-order bending mode for the cross-girder and cross-girder (C-C) combinations and the second-order transverse mode for the hanger member and hanger member (H-H) combinations. The figure also reveals that the stiffening girder and cross girder (G-C) and stiffening girder and hanger member (G-H) combinations exhibited consistency for each pair of damaged members, although the changes were smaller than those for each identical members. Moreover, the cross-girder and hanger-member (C-H) combinations are also consistent within the plane. Nevertheless, it is difficult to classify the damage location using these modes alone because the markers frequently overlap in the same damage member combination.

Figure 11(d) illustrates the relationship between the natural frequencies of the first-

and third-order bending modes. In this figure, there is less overlap between the damage cases of the stiffening girder and hanger member (G-H) and hanger member and hanger member (H-H), with damage cases roughly forming three groups for each damage location. This is likely due to the variation in the natural frequency changes depending on the damage location of the hanger member in the first-order bending mode and that and stiffening girder in the third-order bending mode. This makes the estimation of the damage location relatively straightforward in the case of multiple damage.

However, the damage combinations of Hlb2, Hua3, Hub3, Hlb3, Hua5, Hla6 and Hua5 were plotted at similar locations, making it challenging to determine the damage location. In the damage case of cross girder and cross girder (C-C), the concentration of the plots near the origin indicates a low sensitivity to damage owing to the small changes in both natural vibration modes. In the stiffening girder and cross girder (G-C) and cross girder and hanger member (CH) damage cases, the plots overlapped, and the difference in natural frequencies was small. Consequently, it is difficult to classify the damage to a cross-girder based solely on the bending mode.

Figure 11(e) displays the relationship between the natural frequencies of the second-order transverse mode and the third-order bending mode. It can be observed that the plots for the damage cases in the stiffening girder and cross girder (G-C) have less overlap. This is because of the significant influence of stiffening girder damage on the natural frequency of the third-order bending mode.

The damage cases for the cross girder and cross girder (C-C), stiffening girder and hanger member (G-H), and hanger member and hanger member (H-H) were found to exhibit substantial variation in specific directions. Conversely, the damage cases for the stiffening girder and stiffening girder (G-G) were plotted around the origin, indicating that classification using these natural vibration modes alone is challenging.

As discussed above, we found that changes in the natural frequencies of the modes, characteristic of each member, can be utilised to classify multiple types of damage.

4.3. Damaged member/damage location and angle of rotation

In Section 3.1, it was observed that damages at symmetrical positions show similar changes in natural frequencies, making it difficult to classify the damages. This section examines the classification of these damages using rotation angles.

Figure 13 illustrates the change in rotation angle during damage to Hlb2, Hla6, Hlb3, Hua3, Hub3, and Hua5, which proved difficult to classify based on natural frequency due to the symmetry of the damage locations. Positions 2 and 6, as well as 3 and 5, are symmetrical.

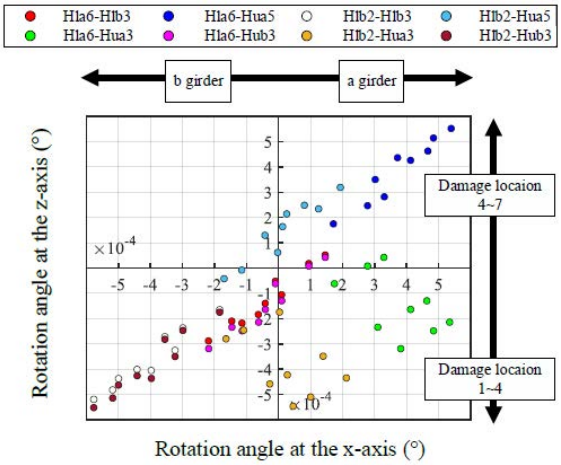

Figure 13　Rotation angle at multiple damage

In the figure, the horizontal axis represents the rotation angle at the x-axis, the vertical axis represents the rotation angle at the z axis, and the colours of the markers indicate different combinations of damage.

Focusing on Hla6-Hua3 (green), both damages involved in a girder, resulting in them being plotted in the region where the rotation angle at the x-axis was significant. On the other hand, in the case of Hla6-Hub3 (pink), where damages involved in both a and b girder, the rotation angle at the x-axis was smaller compared to the green plots and was plotted near the centre. This trend is also evident in the relationships between Hla6-Hua5 (blue) and Hlb2-Hua5 (light blue), as well as between Hlb2-Hlb3 (white) and Hlb2-Hua3 (yellow). The plots of Hla6-Hlb3 (red) and Hla6-Hub3 (pink), as well as Hlb2-Hlb3 (white) and Hlb2-Hub3 (brown), appear to overlap; this is because damages have occurred in the same hanger members.

Hla6-Hua5 (blue), both damages were within the positions 4 to 7, causing the rotation angle at the z-axis to increase in the positive region. Both Hlb2 and hlb3 (white) corresponded to damage positions 1 to 4, causing the rotation angle to increasing significantly in the negative direction. Furthermore, in cases such as Hla6-Hub3 (green), Hlb2Hua5 (light blue), Hla6-Hua3 (pink), where damages occurred in both positions 1 to 4 and 4 to 7, it is observed that they are distributed around the central region. From these trends, the plots in Figure 13 were dispersed into positive and negative regions of x or y-axis, allowing for the classification of each damages.

Indeed, from the above analysis, it can be concluded that even in cases of multiple damages, it is feasible to pinpoint the location of the damaged members by utilising the rotation angle in addition to the natural frequency. Therefore, this method offers a more comprehensive approach for assessing and identifying the severity and location of

damage within a structural system such as a bridge.

5. Conclusion

In this study, damage analysis was conducted on a steel langer arch bridge model, setting single and multiple damages, to investigate the applicability of natural frequency and rotation angle as features that can detect multiple damages, aiming to utilize a small number of sensors in vibration health monitoring. The changes in the mechanical behaviour and vibration characteristics owing to damage were analytically clarified. The results were as follows:

1) By setting damage in the structural model and analysing the subsequent changes in natural frequencies and rotation angles, these features were observed to be sensitive to the location and severity of damage.
2) The stiffening girder is sensitive to the third-order bending mode, the hanger member is sensitive to the first and second-order bending modes, and the cross girder is sensitive to the first and second-order transverse modes.
3) It was also observed that the natural frequencies and rotation angles changed almost linearly with the extent of the damage, suggesting that it is possible to estimate the level of damage by monitoring these changes.
4) In the case of multiple damages, the changes in natural frequencies and rotation angles followed a plane, showing the superposition of the effects of each individual damage. This shows that it is possible to estimate the location and extent of multiple damages by analysing these changes.
5) Even in cases of multiple damages, the combination of changes in natural frequencies and rotation angles can help pinpoint the location of damaged members to some extent.

Acknowledgment

This research received support from the JFE 21st Century Foundation in 2022 through their funding scheme.

References

[1] Road Bureau, Ministry of land, infrastructure and transport document 2 from meeting no. 1 of experts on highway bridge preventive maintenance held october 24, 2007.
[2] M. Greenwood, What Caused Taiwan's Nanfang'ao Bridge to Collapse?, 2019.
[3] Wakayama City, Publication of the investigation committee report concerning the

damage to the musota aqueduct bridge and the aqueduct bridge maintenance and management manual, 2022.

[4] C.-W. Kim, F.-L. Zhang, K.-C. Chang, P. J. McGetrick, Y. Goi, Ambient and vehicle-induced vibration data of a steel truss bridge subject to artificial damage, Journal of Bridge Engineering 26 (2021)

[5] D. M. Siringoringo, Y. Fujino, Estimating bridge fundamental frequency from vibration response of instrumented passing vehicle: Analytical and experimental study, Advances in Structural Engineering 15 (2012) 417 – 433.

[6] A. Furukawa, T. Matsuo, K. Nishikawa, A study on damage detection of the steel truss bridge based on the spectral element method using high frequency excitation, Journal of Japan Society of Civil Engineers, Ser. A1 (Structural Engineering & Earthquake Engineering (SE/EE)) 68 (2012) I_523–I_532.

[7] K. Maes, G. Lombaert, Monitoring railway bridge kw51 before, during, and after retrofitting, Journal of Bridge Engineering 26 (2021).

[8] A. Ruffels, I. Gonzalez, R. Karoumi, Model-free damage detection of a laboratory bridge using artificial neural networks, Journal of Civil Structural Health Monitoring 10 (2020).

[9] K.-C. Chang, C.-W. Kim, Modal-parameter identification and vibration-based damage detection of a damaged steel truss bridge, 636 Engineering Structures 122 (2016) 156–173.

[10] C.-W. Kim, K.-C. Chang, S. Kitauchi, P. J. McGetrick, A field experiment on a steel gerber-truss bridge for damage detection utilizing vehicle-induced vibrations, Structural Health Monitoring 15 (2016) 174 – 192.

[11] A. Ruffels, I. Gonzalez, R. Karoumi, Model-free damage detection of a laboratory bridge using artificial neural networks, Journal of Civil Structural Health Monitoring 10 (2020) 183 – 195.

[12] F. Magalhães, A. Cunha, E. Caetano, Vibration based structural health monitoring of an arch bridge: From automated oma to damage detection, Mechanical Systems and Signal Processing 28 (2012) 212–228. Interdisciplinary and Integration Aspects in Structural Health Monitoring.

[13] S. Donomoto, T. Yamaguchi, T. Kitahara, Damage detection method 650 of steel arch bridge using SOM, Journal of Japan Society of Civil 651 Engineers, Ser. A2 (Applied Mechanics (AM)) 73 (2017) I_813–I_820.

[14] S. G. Lee, G. J. Yun, S. Shang, Reference-free damage detection for 654 truss bridge structures by continuous relative wavelet entropy method, 655 Structural Health Monitoring 13 (2014) 307–320.

[15] L. Zhang, E. J. OBrien, D. Hajializadeh, L. Deng, S. Yin, Bridge damage identification using rotation measurement, Journal of Bridge Engineering 28 (2023).

[16] F. Huseynov, C. Kim, E. OBrien, J. Brownjohn, D. Hester, K. Chang, Bridge damage detection using rotation measurements – experimental 661 validation, Mechanical Systems and Signal Processing 135 (2020).

[17] M.Smith, ABAQUS/Standard User's Manual, Version2022, Dassault Systèmes Simulia Corp, Providence, RI, 2022.

[18] G. Hayashi, R. Oura, A. Hiraoka, T. Yamaguchi, Vibration characteristics and load-carrying capacity of multiple steel plate girder bridges with corroded girder ends, Structure and Infrastructure Engineering (2023) 1–14.